The biogeochemical cycle of iron in the ocean

P. W. Boyd[1]* and M. J. Ellwood[2]

Advances in iron biogeochemistry have transformed our understanding of the oceanic iron cycle over the past three decades: multiple sources of iron to the ocean were discovered, including dust, coastal and shallow sediments, sea ice and hydrothermal fluids. This new iron is rapidly recycled in the upper ocean by a range of organisms; up to 50% of the total soluble iron pool is turned over weekly in this way in some ocean regions. For example, bacteria dissolve particulate iron and at the same time release compounds — iron-binding ligands — that complex with iron and therefore help to keep it in solution. Sinking particles, on the other hand, also scavenge iron from solution. The balance between these supply and removal processes determines the concentration of dissolved iron in the ocean. Whether this balance, and many other facets of the biogeochemical cycle, will change as the climate warms remains to be seen.

Iron is undoubtedly the most studied trace element in the ocean, having received widespread attention since the late 1980s[1,2]. The disproportionate interest in iron stems from the control it was thought to exert on ocean productivity, the resulting sequestration of carbon into the ocean's interior, and consequent modulation of atmospheric carbon dioxide concentrations in the geological past[3]. The iron hypothesis of John Martin[3,4] stimulated new research into iron-enrichment studies[4,5], and so brought a biological component to the emerging discipline of trace metal chemistry[6–8].

In the past 20 years, iron-enrichment experiments ranging from bottle incubations[4,5] to large-scale (50–100 km²) open-ocean amendment studies[9] have demonstrated that iron supply stimulates phytoplankton growth in high-nitrate low-chlorophyll waters, which make up 25% of the world ocean[10]. Iron supply also helps to regulate nitrogen fixation by diazotrophs in nutrient-poor low-latitude waters, according to some modelling studies[11] and field surveys[12]. Taken together with high-nitrate low-chlorophyll regions, iron may control productivity in half of the world ocean[11]. Furthermore, open-ocean amendment studies have revealed the wide-ranging influence of iron supply on key biogeochemical processes, including the drawdown of carbon dioxide from the atmosphere[9,10], the production of dimethyl sulphide[9] and the downward export of particulate organic carbon[13]. Such findings lend support to the suggestion that oceanic iron accounted for up to 25% of the decrease in atmospheric carbon dioxide concentrations during glacial maxima in the geological past[14].

At the same time, trace metal chemists have sought to address the enigma of why iron, the fourth most crustally abundant element[15], is present at vanishingly low concentrations over much of the ocean. Inextricable linkages between iron chemistry and biological processes emerged[7], and it became apparent that interdisciplinary research was essential to develop the fledgling field of ocean iron biogeochemistry.

The thirty-year joint focus on iron chemistry and the influential role of ocean iron enrichment on the carbon cycle has led to rapid and significant advances in our understanding of iron biogeochemistry. Distinct sub-themes have arisen, examining links between biological iron demand and algal physiology, the sources of iron, the role of oceanic circulation and residence time in determining dissolved iron distributions, the function of iron-binding ligands, the fate of particulate iron, and the development of iron biogeochemical budgets and models. Here, we review the oceanic biogeochemical cycle of iron and explore the contribution of these sub-themes to our understanding of this cycle.

Global patterns of ocean iron

The first vertical profiles of 'dissolved' iron (traditionally defined as <0.4 or <0.2 μm filterable iron, but now known to include colloids), to 4 km depth, were published in the 1980s[1,2,8,16]. These detailed profiles were a remarkable achievement, because they overcame significant issues associated with shipboard contamination of water samples and deep-water collection using discrete samplers. In the northeast Pacific, the vertical distribution of iron was characterized by concentrations of ~0.05 nmol Fe l⁻¹ in surface waters, which gradually increased to a maximum of ~0.7 nmol l⁻¹ by 1 km depth and then decreased slightly by 4 km (ref. 2). In other words, the vertical distribution of iron had a nutrient-like profile indicative of its biological role[1] (Fig. 1a).

During the early 1990s, further profiles were published from different ocean basins, including the Atlantic[17] and Indian Oceans[18]. However, it was not until publication in 1997 of 30 profiles — spanning the Pacific, Atlantic and Southern Oceans[19] — that informed debate could proceed regarding the control of dissolved iron concentrations in different ocean basins. A near constancy in deep-water dissolved iron concentrations (~0.7 nmol l⁻¹) was evident in different ocean basins[19]; this concentration exceeded the solubility of iron(III) in seawater (0.08–0.2 nmol l⁻¹)[20,21]. What was more, the shape of most iron profiles resembled that of the major nutrients (phosphate, nitrate and silicate). This trend was at odds with both the short residence time for iron (100–200 years) relative to ocean circulation (1,000 years), and the profiles of other particle-reactive elements with short oceanic residence times, such as lead, which show decreased concentrations with depth[6,19]. It was suggested that the complexation of iron to organic ligands could explain both trends[19].

However, the constancy of deep-water iron concentrations was subsequently called into question, and attributed to the selection of sampling sites[22]. In recent years, further iron profiles[23,24] have revealed considerable inter- and intra-basin variability in dissolved iron concentrations with depth (Supplementary Fig. S1). Such variability may be due to the confounding influence of different analytical methods, the proximity to different iron sources (Fig. 1c and d),

[1]National Institute of Water and Atmosphere Centre of Chemical and Physical Oceanography, Department of Chemistry, University of Otago, Dunedin, New Zealand, [2]Research School of Earth Sciences, The Australian National University, Canberra, ACT 0200 Australia. *e-mail: pboyd@alkali.otago.ac.nz
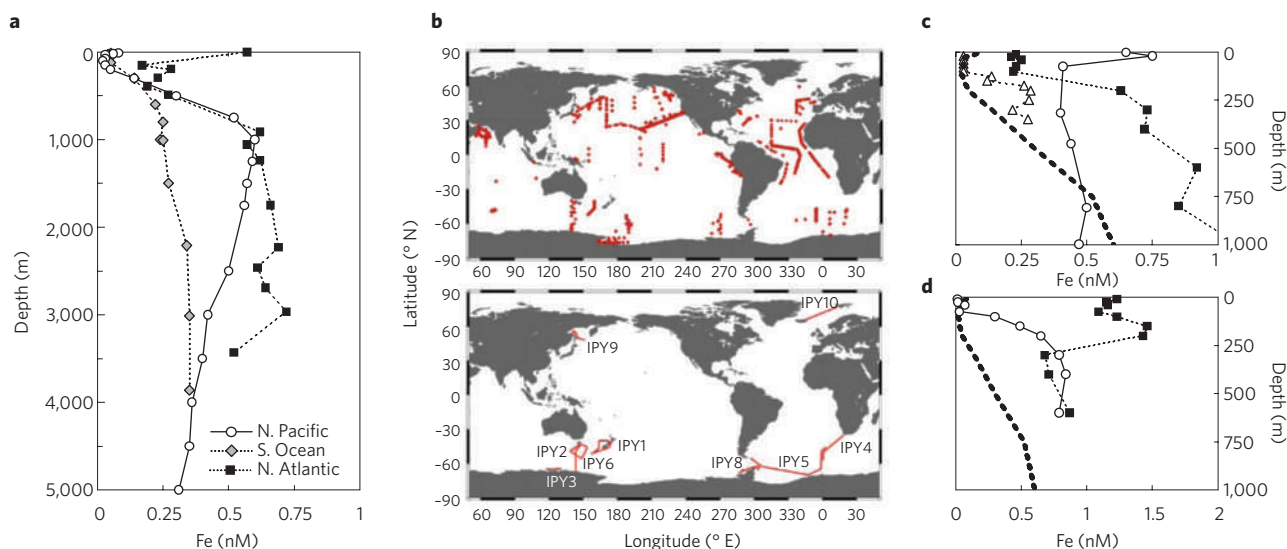
Figure 1 | Dissolved iron vertical profiles illustrating aspects of supply and removal processes. a, Dissolved iron profiles for the north Atlantic[25], central north Pacific[91] and Southern Ocean (A. Bowie, unpublished data) that exhibit representative features for each ocean basin (Supplementary Fig. S1) from regions where SAFe (sampling and analysis of Fe) standardization has taken place (see Supplementary Fig. S2). **b,** Compilation of sampling sites for dissolved iron measurements[44] (upper panel) and recent GEOTRACES International Polar Year oceanographic sections (lower panel). **c,** Iron supply mechanisms in the North Pacific include: lateral advection[26] (filled squares), atmospheric deposition[92] (open circles) and hydrothermal supply[29] (triangles) compared with a 'typical' dissolved iron profile (dashed line)[91]. **d,** Profiles within an anticyclonic mesoscale eddy during formation (filled squares) and 12 months later (open circles)[30] compared with a 'typical' profile (dashed line)[91].
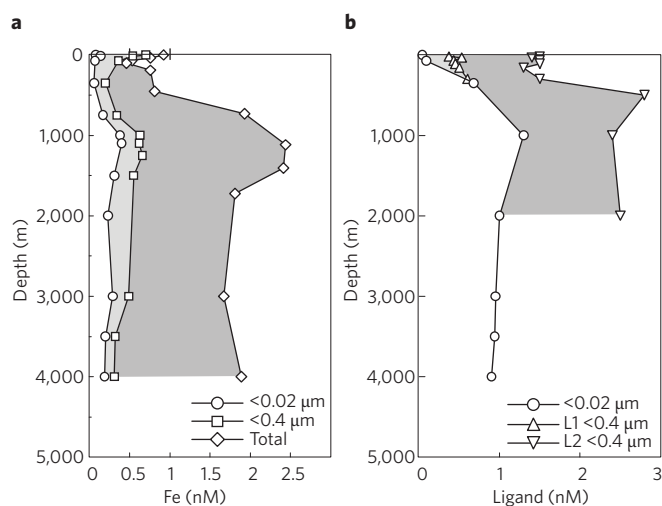
Figure 2 | Size-partitioning of iron and iron-binding ligands with depth. a, Profiles of soluble (<0.02 μm)[21], dissolved (<0.4 μm)[21] and total iron (particulate + dissolved)[92] concentration for the North Pacific. Shaded areas denote colloidal (0.02–0.4 μm) and particulate iron (>0.4 μm). **b,** Profiles of soluble ligand (<0.02 μm)[21] and dissolved (<0.4 μm) ligand (that is, L1 and L2) concentrations[38] for the North Pacific. Shaded area indicates colloidal ligand concentrations[21]. Both profiles were obtained from a site in the vicinity of 23° N 158° W, but in different years.

and the influence of iron-removal processes on water masses as they age[21]. However, statistical analysis of dissolved iron profiles reveals subtle inter-basin differences in deep-water iron concentrations, with slightly higher concentrations in the Atlantic relative to the Pacific and Southern Ocean (Supplementary Figs S1 and 2; Fig. 1a).

Lower iron concentrations in the Pacific Ocean reflect the increasing age of deep water as it moves along global ocean circulation pathways. As waters age, adsorption, precipitation and aggregation processes convert soluble iron into colloidal or particulate

forms, in a process known as scavenging[21,25] (Fig. 1a). Thus 'typical' dissolved iron profiles from the Atlantic, Southern and Pacific Oceans do not show a progressive increase in deep-water concentrations (that is, >2,000 m) with increasing age, as is observed for the major nutrients, which show pronounced enrichment in the deep Pacific Ocean.

Some of the intra-basin variability in dissolved iron concentrations reflects the multiple iron-supply mechanisms present in each basin, and the mismatch between the residence time of iron relative to ocean circulation[19]. For example, coastal sediments influence iron concentrations in the east and west Pacific[1,26] (Fig. 1c), atmospheric dust alters surface iron concentrations in the west and north Pacific[27,28], and hydrothermal inputs modify mid-water iron concentrations along the Equator[29] (Fig. 1c). Newly discovered supply mechanisms, including offshore eddy transport of iron-rich coastal waters, also elevate dissolved iron concentrations in oceanic waters[30] (Fig. 1d). Standardization of iron measurements[31], and the ability to measure iron redox speciation and identify the different chemical properties of each species (Fe(II) has a half-life of minutes to hours)[32], has also improved our understanding of the factors regulating dissolved iron concentrations.

Colloids and ligands

The role of colloids in scavenging iron[21] (Fig. 2a), and elucidation of the vertical distribution of different iron-binding ligands[33], has also enhanced understanding of iron distribution. Two distinct classes of iron-binding ligands, with different affinities for complexing iron, have been identified[33]. Vertical profiles of these ligands differ: the 'strong' iron-binding ligand class (L1) is confined to the upper ocean, whereas the 'weak' iron-binding ligand class (L2) is generally observed throughout the water column (Fig. 2b)[33]. Current evidence suggests that L1 is produced by heterotrophic and autotrophic bacteria to aid iron acquisition, and on the basis of comparable conditional stability constants, the L1 class may be composed largely of siderophores[34]. Degradation products released during the decomposition of organic matter may constitute the L2 class[21,33]. Recent evidence has revealed that L2 are released during bacterial degradation of sinking particles
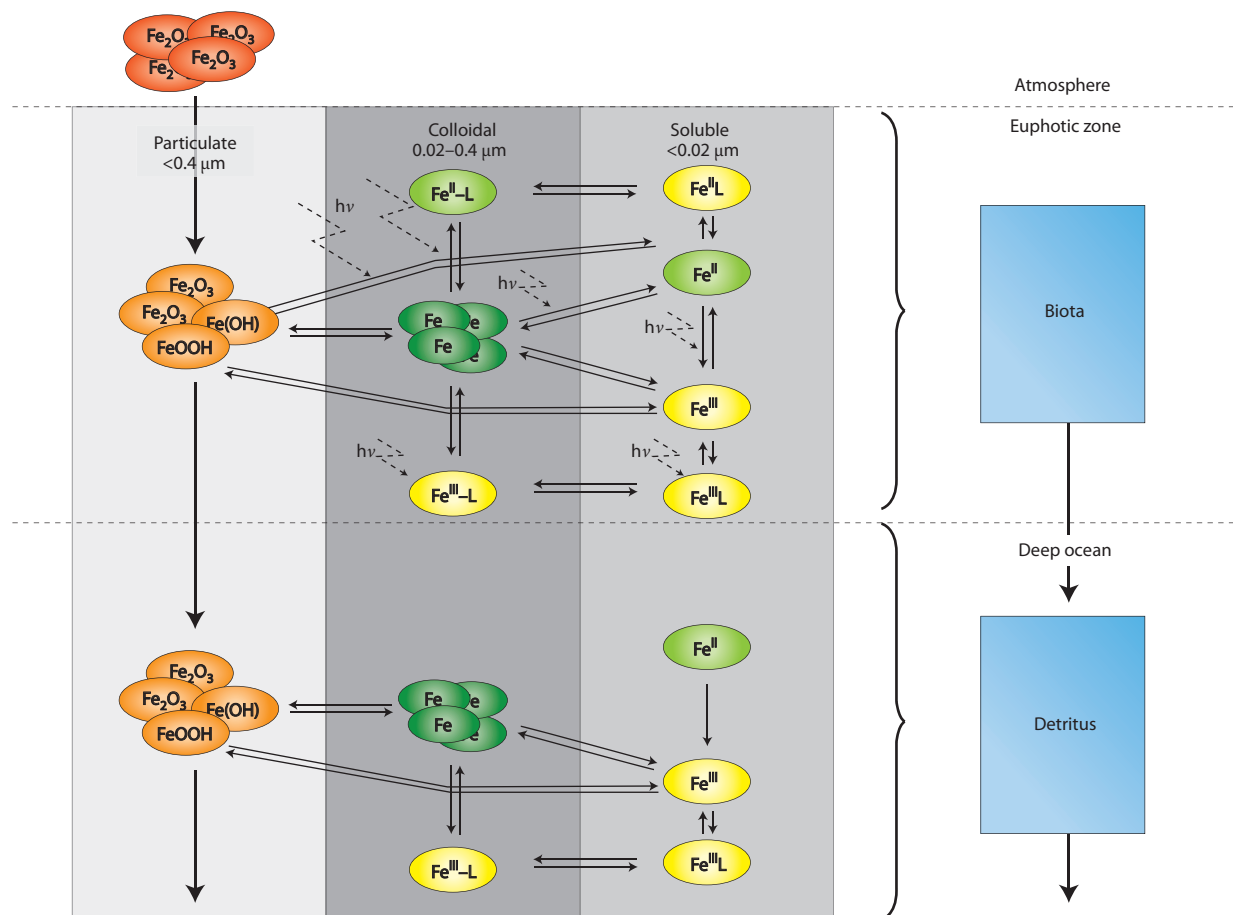
Figure 3 | Modification of aerosol iron upon entering surface waters. Upon deposition, quasi-instantaneous dissolution of aerosol iron (generally <1 to 2%; refs 39,62) is followed by a putative longer-term (weeks) dissolution process (that is, coupled siderophore–photochemical mechanism)[93]. During dissolution most iron probably enters the colloidal pool[40] where it interacts with ligands, although particulate iron can directly enter the soluble pool or be photoreduced (denoted by hv) to Fe(II)[37]. L1 and L2 ligand classes reside in both soluble and colloidal pools[21,38]. In the colloidal phase, dashes between Fe(II) or Fe(III) and L denote uncertainties regarding the type of complexed molecule formed (see Fig. 2). Lithogenic particles settle out after a residence time of weeks to months[94]. Subsurface waters are aphotic and hence there are fewer iron transformation pathways[35].

in subsurface waters[35]. Other L2 sources include highly photoactive siderophores produced by some marine bacteria[36] and photolysis-ligand products of some high-affinity marine siderophores[37]. Although the precise source and identity of these ligands remains elusive, they are thought to play an important role in keeping iron in solution[18,20,33].

A significant portion of iron and iron-binding ligands can reside in both the soluble (<0.02 μm) and colloidal (0.02–0.4 μm) size ranges[21,38]. The vertical distribution of soluble and colloidal iron differs, suggesting different reactivities for each pool[21]. The mixed-layer residence time of iron within these pools varies: soluble iron has a residence time of months to years[25], and colloidal iron has a residence time of months[25]. At present it is unclear what mechanisms influence iron and/or ligand exchange between these pools, but, in the upper ocean, photochemical reduction and biological uptake of iron probably aid its transfer between soluble and colloidal pools (Fig. 3). Aggregation of colloidal material may be assisted by dissolved (<0.2 μm) organic matter as it forms gels and ultimately organic particulates. These particulates will remove iron from the dissolved phase, aiding a redistribution of iron between the soluble and colloidal pools (Fig. 3).

Each dissolved iron profile reflects the dynamic interplay between different supply (Fig. 1c and d) and removal processes. In surface waters, biological uptake decreases concentrations of iron in the soluble (truly dissolved) pool, to levels that do not permit

precipitation of iron hydroxides[20] (Fig. 2a). Under these conditions, ligand complexation of iron released from aerosol-derived lithogenic particulates and colloids can occur, and is aided through photochemical reduction processes[37] (Fig. 3). The proportion of iron released from such lithogenic particulates depends on their mineralogy, in particular how much iron is bound within the aerosol, and subsequent atmospheric and oceanic processing[39].

Below the surface mixed layer, sinking detrital matter is biologically degraded and transformed, releasing iron and organic ligands[35] into the soluble and colloidal pools. Complexation by natural ligands, and scavenging by sinking particles, compete for the iron as it enters these pools following particle breakdown[40] (Fig. 3). Complexation will tend to increase dissolved iron concentrations, whereas scavenging will lower concentrations. Particles and colloids[21] that scavenge iron may then aggregate with other colloids and particles and settle to the sea floor. The reactivity of iron in both the soluble and colloidal pools in the upper and subsurface ocean has important implications for the dissolution of aerosol dust, the acquisition and recycling of iron by biota, and the remineralization and scavenging of iron (Fig. 3). The interplay between these processes is explored in the following sections.

Iron supply

Iron supply terms can be divided into new (that is, adding to the oceanic inventory) and recycled (turnover of the inventory). Here
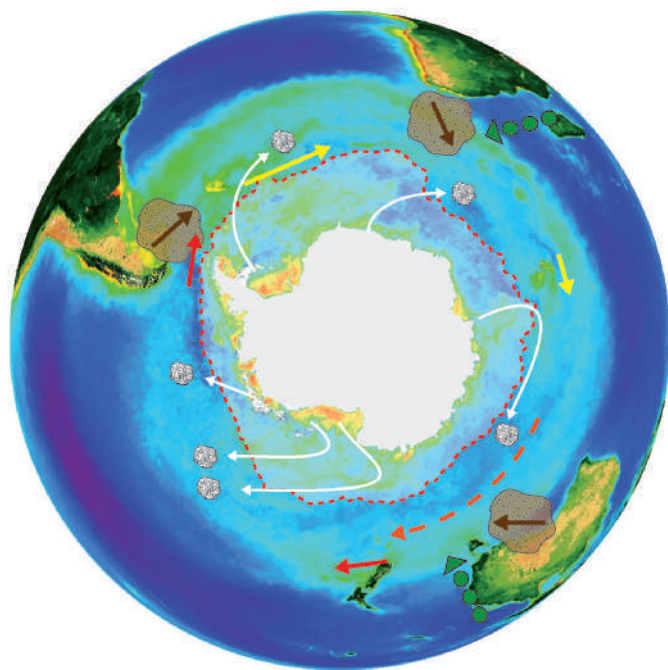
Figure 4 | Multiple sources of new iron to the Southern Ocean. Illustrative examples of sources (arrows) are overlaid on an annual composite of satellite ocean colour (a proxy for phytoplankton stocks; warmer colours denote higher stocks). The main supply mechanisms are: dust deposition (brown symbols), island-wake effects (yellow arrows), iceberg drift and melt (white trajectories/symbols), seasonal ice-melt (red circumpolar dashed line), lateral transport of iron-rich sediments (red arrows), eddy shedding/sediment entrainment (green symbols) and bathymetric interactions with the Antarctic Circumpolar Current (dark orange dashed arrow) which uplift iron-rich waters by up to 100 m (based on modelling simulations; S. Solokov and S. Rintoul, personal communication). Image courtesy of NASA and Orbimage.

we focus on new iron. Atmospheric dust is a key supply term in the northeast subarctic Pacific[1,2]. The first global maps of aerosol iron flux to the ocean were based on studies such as the SEAREX (Sea Air Exchange) aerosol sampling network[41,42]. These maps revealed strong aerosol flux gradients both zonally, for example from west to east in the north Pacific Ocean, and meridionally, for example north to south in the Indian Ocean. These gradients were linked to the location of arid regions, and to the distance between the dust source and sink in the ocean (half of the atmospheric dust load is lost through oceanic deposition on a length scale of <1,500 km; ref 41). Dust supply maps also revealed that remote high-nitrate low-chlorophyll waters such as the Southern Ocean are characterized by particularly low aerosol-iron fluxes, and hence provided a strong semi-quantitative causal link between low iron supply and low ocean productivity[42].

Construction of preliminary iron budgets for the Southern Ocean suggested that, unlike in the northeast subarctic Pacific[1,2], upwelling of iron-rich waters supplies much of the iron[43]. In fact, there are multiple sources of new iron in the Southern Ocean, which show different temporal signatures (that is, seasonal to episodic) and spatial gradients (that is, meridional to zonal, Fig. 4). Iron sources include resuspension of coastal and shallow sediments[44], glacial/iceberg melt[45], seasonal sea-ice retreat[46], dust[42], hydrothermal activity[47], eddy shedding/sediment interactions[48], island wakes[49], vertical diffusive flux[50], volcanism[51] and the interaction between the bathymetry and currents (termed bottom pressure torque[52]). The cumulative influence of these sources is evident in an annual Southern Ocean

composite for satellite-derived ocean colour (Fig. 4). This 'variegated ocean' reveals both regional hotspots and pronounced meridional and zonal gradients in phytoplankton stocks.

Further iron sources are evident in other oceanic regions. In coastal waters, both sedimentary[53,54] and riverine[55] iron cause pronounced nearshore to offshore gradients in dissolved iron concentrations[56]. Although riverine iron is an important supply term at source[57], much of the incoming iron is rapidly scavenged, for example by salt-induced flocculation, onto settling particles in estuaries[58]; the remainder probably contributes to the shelf iron inventory. And iron from arid regions is not the only aerosol source; extraterrestrial dust[59] and iron-rich particles from urban pollution[60] and biomass burning[61] also contribute. The complex range of iron-containing aerosols may explain much of the observed variability in aerosol solubility in dissolution studies[39,62], which represents a large uncertainty in global iron budgets[63]. Together, these multiple sources form a mosaic of iron supply mechanisms, both regionally and globally. A key challenge will be to resolve how the magnitude of these different supply modes alters with both inter-annual variability and a sustained change in climate.

The ferrous wheel

Although much research has focused on documenting the source of new iron, it is now evident that, as for other important nutrients, ocean biota play a pivotal role in recycling iron. Thus, although iron supply limits primary productivity in much of the ocean[11], the recycling of dissolved iron is biologically mediated[64]. It has long been established that phytoplankton require iron for growth[65]. But the provenance of the acquired iron was poorly constrained, and the relative role of the microbial food web in iron recycling unresolved. In the 1990s, studies highlighted the role of bacteria and grazers in regenerating iron[66,67], and initial biological iron budgets revealed a balance between iron uptake and subsequent recycling[64]. This cycle of rapid iron uptake and regeneration was termed the ferrous wheel[68] (Fig. 5a).

Biological iron uptake is driven by a range of mechanisms, which can be broadly split between prokaryotes and eukaryotes (Fig. 5a). Heterotrophic and autotrophic bacteria (prokaryotes) acquire iron using siderophore-based iron transport systems[69,70]; the former also possess inorganic iron transport systems[36] to access other forms of iron under iron-replete conditions. Siderophores are chelators released by bacteria — generally under iron-limiting conditions — that strongly bind ferric iron, and can solubilize it from a range of particles and minerals[71]. In contrast, eukaryotes, such as diatoms, have not been shown to produce siderophores. For some time they were thought to use dissolved inorganic Fe(III)′ species directly from solution (the Fe′ model)[72] (Fig. 5a). However, it was later discovered that soluble iron must be reduced before being taken up[73]. Iron-reducing enzymes — present in the membranes of eukaryotes — are responsible for iron reduction. The greater bioavailability of Fe(III)′ species can be attributed to the high rates, relative to ferric chelates, with which they are reduced by these enzymes[73]. Algal cell size has a marked influence on the rate of extracellular iron reduction: smaller cells reduce iron at higher rates per unit biomass[71]. Mixotrophic phytoplankton, for example photosynthetic flagellates that ingest bacteria, are reported to use colloidal iron directly[74] (Fig. 5a).

The pool of particulate biogenic iron in surface waters is rapidly recycled by microzooplankton (both grazers[75,76] and mixotrophs[77]), mesozooplankton[66,78], viruses[79] and heterotrophic bacteria[75]. Thus the ferrous wheel rapidly mobilizes the biogenic iron pool, making it bioavailable[75]. The makeup of the ferrous wheel varies with region[75,78], and depends on the partitioning of iron between biogenic pools (Fig. 5b). The contribution of new iron to total iron supply — the *fe* ratio (new iron/(new + regenerated iron))[50] — ranges from 10% in high-nitrate low-chlorophyll waters[50] to 50% in high-iron
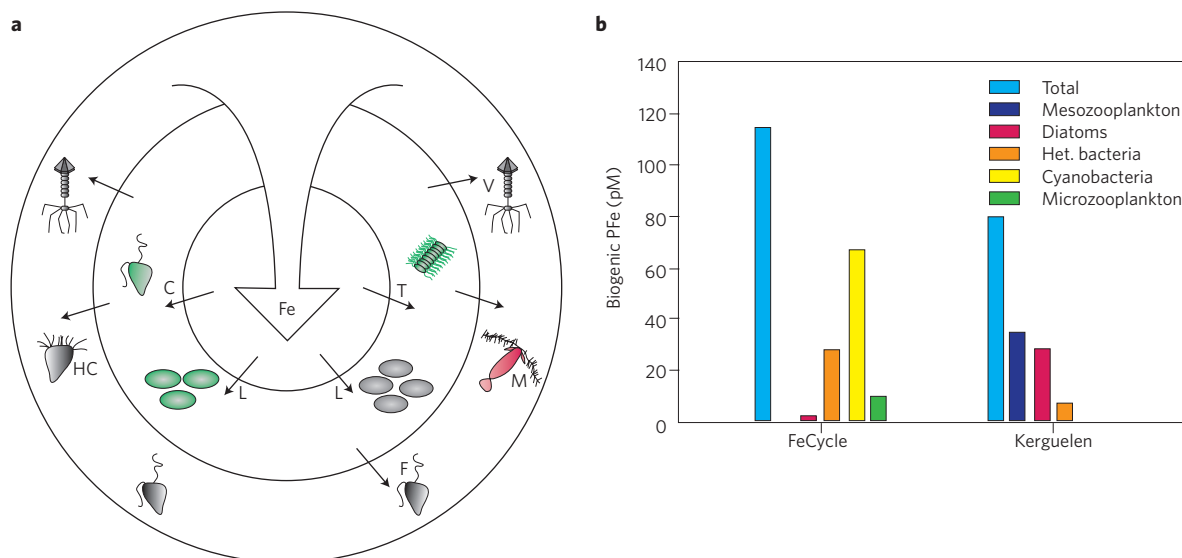
Figure 5 | Biological iron recycling in the upper ocean. a, Schematic of the microbial ferrous wheel which drives pelagic iron recycling. 'Fe' represents a generic pool of inorganic and organic, soluble, colloidal and particulate iron that is potentially available to biota. Iron acquisition strategies include: siderophore-mediated uptake (L), direct colloidal iron uptake (C) and dissolved iron uptake (T). After uptake, iron is rapidly cycled by heterotrophic flagellates (F), ciliates (HC), mesozooplankton (M) and viral lysis (V). **b**, The partitioning of particulate biogenic iron (PFe) in surface waters for two contrasting Southern Ocean sites: FeCycle (*fe* ratio = 0.1)[50] versus Kerguelen (*fe* ratio = 0.5)[80,84].

waters[78]. The size of the ferrous wheel varies with depth: larger biogenic iron pools are found in surface waters, relative to those found in subsurface waters, where iron regeneration is up to tenfold slower, probably owing to lower microbial biomass[35] and a reduction in the availability of bacterial substrates with depth.

The fate of particulate iron

As iron-containing particles sink to the ocean interior, iron gradually undergoes remineralization. As a result, iron is released into soluble and colloidal pools, and the deep-water inventory is replenished (Figs 3 and 6). The highest particulate fluxes are just below the surface mixed layer, and decrease with depth owing to iron remineralization (Fig. 6a)[80,81]. Thus the greatest attenuation of particulate iron flux, and hence the highest rates of iron remineralization, takes place in the upper ocean, and decreases progressively with depth. However, a comparison of vertical trends in particulate iron flux and dissolved iron concentrations (Fig. 6) reveals a mismatch between increases in dissolved iron concentrations, and decreases in flux attenuation, with depth. Three distinct strata are evident, commencing with the upper 250 m where dissolved iron is generally low (<0.1 nmol l^{-1}). In contrast, between 250 and 1,000 m depth, there is a pronounced increase in dissolved iron. Below 1,000 m a small but significant decrease in dissolved iron concentration is evident (Fig. 6c).

This mismatch indicates that remineralization alone does not control dissolved iron concentrations. Remineralization of particulate iron, for example by heterotrophic bacteria, seems to exert more control over dissolved iron concentrations between 250 and 1,000 m depth than the scavenging of dissolved iron by sinking particles[40]. The opposite seems to be true below 1,000 m depth[40] (Figs 6b and 6c). However, the relative role of particle remineralization versus scavenging in the upper 250-m stratum is less clear. Here, decreases in particulate iron flux are observed, but no obvious increase in dissolved iron concentrations is evident (Supplementary Fig. S3).

The trends in dissolved iron concentrations in the upper 250 m in low-latitude waters are probably owing to the interplay between iron inputs from dissolution of terrestrial aerosols, such as desert dust near the sea surface, and biological uptake within the euphotic zone[50], which may be especially heightened within the deep chlorophyll maximum[82] (DCM, ~120 m depth,

Supplementary Fig. S3). These combined processes can generate maxima at the sea surface and minima within the deep chlorophyll maximum[27,82], which confounds identification of the depth at which net particulate iron dissolution commences. There are several potential explanations for trends observed in this stratum (see Supplementary Information).

Multiple factors may determine the relative influence of remineralization and scavenging in the upper 250 m of the ocean. These include the aggregation of colloidal iron and its enhanced settling as it aggregates with large particles[21], the release of both iron and L2 into both the soluble and colloidal pools from detritus during remineralization[35,38], rapid vertical attenuation of some components of the settling particulate iron flux (iron in settling algal cells is generally more labile than that in lithogenic mineral phases)[35], and/or the sorption of dissolved iron onto the particles from which it was previously remineralized[80]. Recent studies of detailed particle profiles from the open ocean reveal more than a tenfold decrease in the total surface area of sinking particles at a depth of 50 m below the surface mixed layer (G. Jackson, personal communication). This is likely to have important ramifications for the biological recycling of a particle-reactive element such as iron.

More research is required to explain the factors responsible for preventing more immediate remineralization of settling particulate iron, relative to other elements (see Fig. 6a), in subsurface waters. One important implication of delayed remineralization of iron is that in some regions the ferricline (the boundary between low-iron surface and high-iron deeper waters) is deeper than the nutricline[19,80]. Such a mismatch in the depth of the ferricline and nutricline alters the iron and nutrient stoichiometry of water supplied to the upper ocean, causing iron limitation of new production.

Budgets and biogeochemical models

Early attempts to develop oceanic iron budgets focused on geochemical aspects and relied on a wide range of assumptions[2,43]. These simple geochemical budgets demonstrated that the dominant supply mechanism for new iron varies between regions. Initial biological budgets[64] revealed the rapid uptake and subsequent recycling of iron, but offered little insight into how the supply of new iron helped to structure such budgets. The first budget to combine
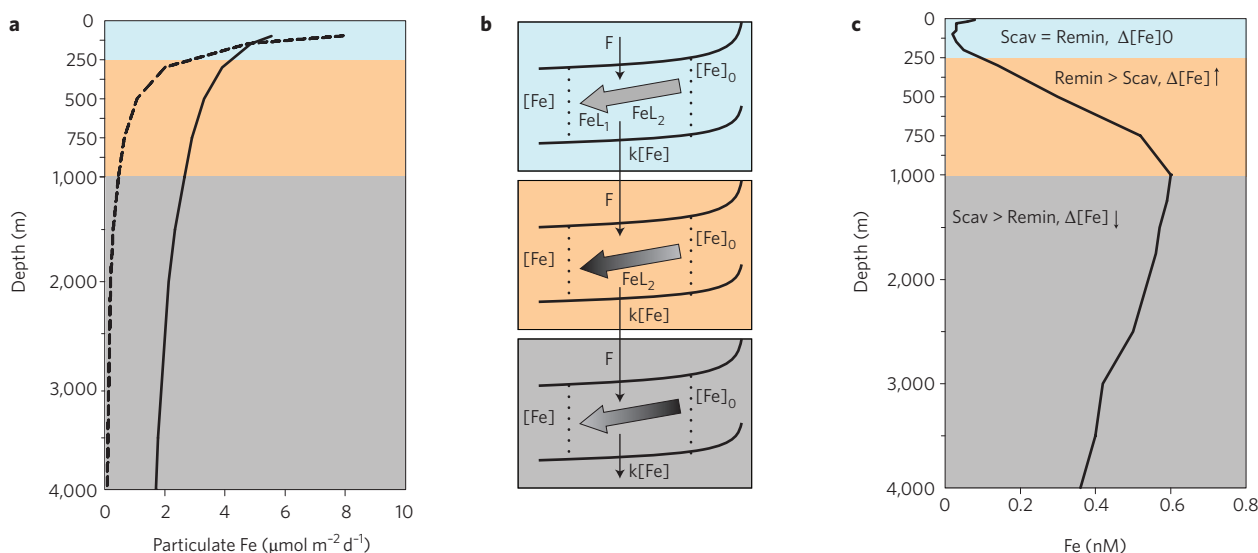
Figure 6 | The influence of particle scavenging and remineralization on dissolved iron concentrations in three zones (0–250 m (blue), 250–1,000 m (orange) and >1,000 m (grey)) denoted in panels a–c. a, Attenuation of particulate iron export flux (150–500 m depth; solid curve)[81] is contrasted with predicted iron export flux based on the particulate organic carbon export flux (150–500 m depth; dashed curve) and an Fe:C molar ratio of 3.3 mmol:mol (ref. 81)) projected to 4,000 m. **b**, Modified 'pipe diagram' of the effect of scavenging versus remineralization on the dissolved iron concentration of a water parcel transiting an isopycnal surface (solid black curve). F denotes the dissolution of iron from settling particles (downward arrows); k[Fe] represents iron removal from the dissolved phase through scavenging. $[Fe]_0$ is the initial dissolved iron concentration on the isopycnal and [Fe] represents the final iron concentration along the isopycnal. FeL_1 and FeL_2 denote the release of 'strong' and 'weak' iron-binding ligand class, respectively. The thick quasi-horizontal arrows represent the movement of the water parcel along as isopycnal. Darker shades along the arrow represent increased dissolved iron concentrations and vice versa. Modified from ref. 40, © 2002 AGU. **c**, A typical dissolved iron profile for the North Pacific[91] overlaid with the relative influences of scavenging (Scav) and remineralization (Remin). Δ[Fe] represents a change (0 no change; upward arrow, increase) in dissolved iron concentration.

geochemical and biological processes, and compare the supply of new versus recycled iron, focused on a mesoscale iron-enrichment experiment[83]. Not surprisingly, the largest budget term was for new iron — the deliberate addition of tonnes of iron salt to the high-nitrate low-chlorophyll water patch. Several recent biogeochemical budgets have attempted a more complete inventory of new and recycled iron pools and fluxes in both low (site of FeCycle study[50]) and high-iron (Kerguelen[84]) waters. Biological aspects of the resulting budgets are compared in Fig. 5b. In iron-replete waters, diatoms and copepods make a much greater contribution to the biogenic particulate iron pool than in low-iron waters, where the microbial community of small cells makes the largest contribution.

Modelling of iron biogeochemistry commenced in the mid-1990s. Relatively simple one-dimensional models were used to predict vertical profiles of dissolved iron, for example based on the remineralization of sinking particulate organic carbon[19]. Since then, there has been an increase in the sophistication and scope of the iron cycling models[85], with three-dimensional models now being routinely run[11,86,87]; a relatively simple iron geochemistry model is coupled to an ocean circulation model, and a three-dimensional field of dissolved iron distributions is simulated. A comparison of model outputs with observations provides a robust test of the assumptions and precepts of the model. Early models pointed to the need to reduce uncertainties in the role of iron-binding ligands[86]. Subsequent models have incorporated different representations of iron-binding ligands, and their dynamics in relation to remineralization, adsorption, desorption and scavenging[87]. However, so far only one ligand class has been successfully represented in such three-dimensional models[87].

Improvements in the representation of iron biogeochemistry in models is essential if we are to better understand how large-scale ocean perturbations, such as those proposed by basin-scale iron fertilization, will alter the biogeochemical cycling of iron, for example remineralization[88].

Ocean iron and climate

How climate change will alter the biogeochemical cycling of iron remains an open question. Climate-mediated changes to oceanic or atmospheric dynamics, for example circulation, may alter both regional iron budgets and the iron inventory of the global ocean. A change in iron supply will, in turn, alter ocean productivity and elemental cycles, for example by enhancing or reducing phosphorus and silicon stocks. Assessing how climate will impact the oceanic iron cycle is hampered by many uncertainties. In particular, the processes underlying the transfer of iron between soluble and colloidal phases[21,40], and the factors controlling the interplay between particulate and dissolved iron in the upper ocean, represent important uncertainties. The rapidly developing field of iron stable isotopic analysis[89,90], together with the launch of a decade-long global survey of trace elements and their isotopes (GEOTRACES; www.geotraces.org), should provide the accuracy and detail necessary to address many of these issues.

References

1. Martin, J. H. & Gordon, R. M. Northeast Pacific iron distributions in relation to phytoplankton productivity. *Deep Sea Res. A. Oceanogr. Res. Papers* **35,** 177–196 (1988).
2. Martin, J. H., Gordon, R. M., Fitzwater, S. & Broenkow, W. W. VERTEX: Phytoplankton/iron studies in the Gulf of Alaska. *Deep Sea Res. A. Oceanogr. Res. Papers* **36,** 649–680 (1989).
3. Martin, J. H. Glacial–interglacial CO_2 change: the iron hypothesis. *Paleoceanography* **5,** 1–13 (1990).
4. Martin, J. H. & Fitzwater, S. E. Iron-deficiency limits phytoplankton growth in the Northeast Pacific Subarctic. *Nature* **331,** 341–343 (1988).
5. de baar, H. J. W. *et al.* On iron limitation of the Southern Ocean — experimental-observations in the Weddell and Scotia Seas. *Mar. Ecol. Prog. Ser.* **65,** 105–122 (1990).
6. Schaule, B. K. & Patterson, C. C. Lead concentrations in the northeast Pacific: evidence for global anthropogenic perturbations. *Earth Planet. Sci. Lett.* **54,** 97–116 (1981).

7. Bruland, K. W., Donat, J. R. & Hutchins, D. A. Interactive influences of bioactive trace metals on biological production in oceanic waters. *Limnol. Oceanogr.* **36,** 1555–1577 (1991).

8. Gordon, R. M., Martin, J. H. & Knauer, G. A. Iron in northeast Pacific waters. *Nature* **299,** 611–612 (1982).

9. Boyd, P. W. *et al.* Mesoscale iron enrichment experiments 1993–2005: synthesis and future directions. *Science* **315,** 612–617 (2007).

10. de Baar, H. J. W. *et al.* Synthesis of iron fertilization experiments: from the Iron Age in the Age of Enlightenment. *J. Geophys. Res. Oceans* **110,** C09S16 (2005).

11. Moore, J. K., Doney, S. C., Glover, D. M. & Fung, I. Y. Iron cycling and nutrient-limitation patterns in surface waters of the World Ocean. *Deep-Sea Res.* **49,** 463–507 (2001).

12. Moore, C. M. *et al.* Large-scale distribution of Atlantic nitrogen fixation controlled by iron availability. *Nature Geosci.* **2,** 867–871 (2009).

13. Boyd, P. W. *et al.* The decline and fate of an iron-induced subarctic phytoplankton bloom. *Nature* **428,** 549–553 (2004).

14. Sigman, D. M. & Boyle, E. A. Glacial/interglacial variations in atmospheric carbon dioxide. *Nature* **407,** 859–869 (2000).

15. Wedepohl, K. H. The composition of the continental crust. *Geochim. Cosmochim. Acta* **59,** 1217–1232 (1995).

16. Landing, W. M. & Bruland, K. W. The contrasting biogeochemistry of iron and manganese in the Pacific Ocean. *Geochim. Cosmochim. Acta* **51,** 29–43 (1987).

17. Martin, J. H., Fitzwater, S. E., Gordon, R. M., Hunter, C. N. & Tanner, S. J. Iron, primary production and carbon nitrogen flux studies during the JGOFS North Atlantic Bloom Experiment. *Deep-Sea Res.* **40,** 115–134 (1993).

18. Kuma, K., Nishioka, J. & Matsunaga, K. Controls on iron(III) hydroxide solubility in seawater: the influence of pH and natural organic chelators. *Limnol. Oceanogr.* **41,** 396–407 (1996).

19. Johnson, K. S., Gordon, R. M. & Coale, K. H. What controls dissolved iron concentrations in the world ocean? *Mar. Chem.* **57,** 137–161 (1997).

20. Liu, X. & Millero, F. J. The solubility of iron in seawater. *Mar. Chem.* **77,** 43–54 (2002).

21. Wu, J. F., Boyle, E., Sunda, W. & Wen, L. S. Soluble and colloidal iron in the oligotrophic North Atlantic and North Pacific. *Science* **293,** 847–849 (2001).

22. Boyle, E. What controls dissolved iron concentrations in the world ocean? A comment. *Mar. Chem.* **57,** 163–167 (1997).

23. de Baar, H. J. W. & de Jong, J. T. M. in *The Biogeochemistry of Iron in Seawater* Vol. 7 (eds Turner, D. R. & Hunter, K. A.) (Wiley, 2001).

24. Measures, C. I., Landing, W. M., Brown, M. T. & Buck, C. S. High-resolution Al and Fe data from the Atlantic Ocean CLIVAR-CO$_2$ Repeat Hydrography A16N transect: Extensive linkages between atmospheric dust and upper ocean geochemistry. *Glob. Biogeochem. Cycles* **22,** GB1005 (2008).

25. Bergquist, B. A., Wu, J. & Boyle, E. A. Variability in oceanic dissolved iron is dominated by the colloidal fraction. *Geochim. Cosmochim. Acta* **71,** 2960–2974 (2007).

26. Nishioka, J., Takeda, S., Wong, C. S. & Johnson, W. Size-fractionated iron concentrations in the northeast Pacific Ocean: distribution of soluble and small colloidal iron. *Mar. Chem.* **74,** 157–179 (2001).

27. Bruland, K. W., Orians, K. J. & Cowen, J. P. Reactive trace metals in the stratified Central North Pacific. *Geochim. Cosmochim. Acta* **58,** 3171–3182 (1994).

28. Brown, M. T., Landing, W. M. & Measures, C. I. Dissolved and particulate Fe in the western and central North Pacific: results from the 2002 IOC cruise. *Geochem. Geophys. Geosyst.* **6,** Q10001 (2005).

29. Gordon, R. M., Coale, K. H. & Johnson, K. S. Iron distributions in the equatorial Pacific: implications for new production. *Limnol. Oceanogr.* **42,** 419–431 (1997).

30. Johnson, W. K., Miller, L. A., Sutherland, N. E. & Wong, C. S. Iron transport by mesoscale Haida eddies in the Gulf of Alaska. *Deep-Sea Res. II* **52,** 933–953 (2005).

31. Johnson, K. S. *et al.* Developing standards for dissolved iron in seawater. *Eos* **88,** 131–132 (2007).

32. Millero, F. J., Sotolongo, S. & Izaguirre, M. The oxidation kinetics of Fe(II) in seawater. *Geochim. Cosmochim. Acta* **51,** 793–801 (1987).

33. Rue, E. L. & Bruland, K. W. Complexation of iron(III) by natural organic ligands in the Central North Pacific as determined by a new competitive ligand equilibration/adsorptive cathodic stripping voltammetric method. *Mar. Chem.* **50,** 117–138 (1995).

34. Mawji, E. *et al.* Hydroxamate siderophores: Occurrence and importance in the Atlantic Ocean. *Envir. Sci. Technol.* **42,** 8675–8680 (2008).

35. Boyd, P. W., Ibisanmi, E., Sander, S., Hunter, K. A. & Jackson, G. A. Remineralization of upper ocean particles: implications for iron biogeochemistry. *Limnol. Oceanogr.* **55,** 1271–1288 (2010).

36. Amin, S. A. *et al.* Photolysis of iron-siderophore chelates promotes bacterial-algal mutualism. *Proc. Natl Acad. Sci. USA* **106,** 17071–17076 (2009).

37. Barbeau, K. A., Rue, E. L., Bruland, K. W. & Butler, A. Photochemical cycling of iron in the surface ocean mediated by microbial iron(III)-binding ligands. *Nature* **413,** 409–413 (2001).

38. Cullen, J. T., Bergquist, B. A. & Moffett, J. W. Thermodynamic characterization of the partitioning of iron between soluble and colloidal species in the Atlantic Ocean. *Mar. Chem.* **98,** 295–303 (2006).

39. Baker, A. R. & Croot, P. L. Atmospheric and marine controls on aerosol iron solubility in seawater. *Mar. Chem.* **120,** 4–13 (2010).

40. Wu, J. F. & Boyle, E. A. Iron in the Sargasso Sea: implications for the processes controlling dissolved Fe distribution in the ocean. *Glob. Biogeochem. Cycles* **16,** 1086 (2002).

41. Prospero, J., Uematsu, M. & Savoie, D. in *Chemical Oceanography* Vol. 10 (ed. Riley, J. P.) 187–218 (Academic, 1989).

42. Duce, R. A. & Tindale, N. W. Atmospheric transport of iron and its deposition in the ocean. *Limnol. Oceanogr.* **36,** 1715–1726 (1991).

43. de Baar, H. J. W. *et al.* . Importance of iron for plankton blooms and carbon dioxide drawdown in the Southern Ocean. *Nature* **373,** 412–415 (1995).

44. Moore, J. K. & Braucher, O. Sedimentary and mineral dust sources of dissolved iron to the world ocean. *Biogeosciences* **5,** 631–656 (2008).

45. Smith, J. *et al.* Free-drifting icebergs: hot spots of chemical and biological enrichment in the Weddell Sea. *Science* **317,** 478–482 (2007).

46. Lannuzel, D. *et al.* Iron study during a time series in the western Weddell pack ice. *Mar. Chem.* **108,** 85–95 (2008).

47. Klunder, P., Laan, P., Middag, R., de Baar, H. J. W. & van Ooijen, J. Dissolved iron in the Southern Ocean (Atlantic Sector) *Deep-Sea Res. II:* (in press).

48. Bowie, A. R. *et al.* Biogeochemical iron budgets of the Southern Ocean south of Australia: decoupling of iron and nutrient cycles in the subantarctic zone by the summertime supply. *Glob. Biogeochem. Cycles* **23,** GB4034 (2009).

49. Blain, S. *et al.* Effect of natural iron fertilization on carbon sequestration in the Southern Ocean. *Nature* **446,** 1070–1074 (2007).

50. Boyd, P. W. *et al.* FeCycle: Attempting an iron biogeochemistry budget from a mesoscale SF$_6$ tracer experiment in unperturbed low iron waters. *Glob. Biogeochem. Cycles* **19,** GB4S20 (2005).

51. Gaiero, D. M., Probst, J. L., Depetris, P. J., Bidart, S. M. & Leleyter, L. Iron and other transition metals in Patagonian riverborne and windborne materials: geochemical control and transport to the southern South Atlantic Ocean. *Geochim. Cosmochim. Acta* **67,** 3603–3623 (2003).

52. Sokolov, S. & Rintoul, S. R. On the relationship between fronts of the Antarctic Circumpolar Current and surface chlorophyll concentrations in the Southern Ocean. *J. Geophys. Res.* **112,** C07030 (2007).

53. Elrod, V. A., Berelson, W. M., Coale, K. H. & Johnson, K. S. The flux of iron from continental shelf sediments: a missing source for global budgets. *Geophys. Res. Lett.* **31,** L12307 (2004).

54. Johnson, K. S., Chavez, F. P. & Friederich, G. E. Continental-shelf sediments as a primary source of iron for coastal phytoplankton. *Nature* **398,** 697–700 (1999).

55. Wetz, M. S., Burke, H., Chase, Z., Wheeler, P. A. & Whitney, M. M. Riverine input of macronutrients, iron, and organic matter to the coastal ocean off Oregon, USA, during the winter. *Limnol. Oceanogr.* **51,** 2221–2231 (2006).

56. Nishioka, J. *et al.* Iron supply to the western subarctic Pacific: Importance of iron export from the Sea of Okhotsk. *J. Geophys. Res.* **112,** C10012 (2007).

57. Mackenzie, F. T., Lantzy, R. & Paterson, V. Global trace metal cycles and predictions. *J. Int. Assoc. Math. Geol.* **11,** 99–142 (1979).

58. Boyle, E. A., Edmond, J. M. & Sholkovitz, E. R. Mechanism of iron removal in estuaries. *Geochim. Cosmochim. Acta* **41,** 1313–1324 (1977).

59. Johnson, K. S. Iron supply and demand in the upper ocean: is extraterrestrial dust a significant source of bioavailable iron? *Glob. Biogeochem. Cycles* **15,** 61–63 (2001).

60. Sedwick, P. N., Sholkovitz, E. R. & Church, T. M. Impact of anthropogenic combustion emissions on the fractional solubility of aerosol iron: evidence from the Sargasso Sea. *Geochem. Geophys. Geosyst.* **8,** Q10Q06 (2007).

61. Luo, C. *et al.* Combustion iron distribution and deposition. *Global Biogeochem. Cycles* **22,** GB1012 (2008).

62. Boyd, P. W., Mackie, D. S. & Hunter, K. A. Aerosol iron deposition to the surface ocean: modes of iron supply and biological responses. *Mar. Chem.* **120,** 128–143 (2010).

63. Jickells, T. D. *et al.* Global iron connections between desert dust, ocean biogeochemistry, and climate. *Science* **308,** 67–71 (2005).

64. Price, N. M. & Morel, F. M. M. in *Iron Transport and Storage in Microorganisms, Plants, and Animals* Vol. 35 *Metal Ions in Biological Systems*, 1–36 (CRC, 1998).

65. Brand, L. E., Sunda, W. G. & Guillard, R. R. L. Limitation of marine phytoplankton reproductive rates by zinc, manganese, and iron. *Limnol. Oceanogr.* **28,** 1182–1198 (1983).

66. Hutchins, D. A. & Bruland, K. W. Grazer-mediated regeneration and assimilation of Fe, Zn and Mn from planktonic prey. *Mar. Ecol. Progr. Ser.* **110,** 259–269 (1994).

67. Lee, B-G. & Fisher, N. S. Release rates of trace elements and protein from decomposing planktonic debris. 1. Phytoplankton debris. *J. Plankt. Res.* **51,** 391–421 (1993).

68. Kirchman, D. L. Microbial ferrous wheel. *Nature* **383,** 303–304 (1996).

69. Haygood, M. G., Holt, P. D. & Butler, A. Aerobactin production by a planktonic marine *Vibrio* sp. *Limnol. Oceanogr.* **38,** 1091–1097 (1993).

70. Wilhelm, S. W. The ecology of cyanobacteria in iron-limited environments: a review of physiology and implications for aquatic environments. *Aquat. Microb. Ecol.* **9,** 295–303 (1995).

71. Sunda, W. G. in *The Biogeochemistry of Iron in Seawater* (eds Turner, D. R. & Hunter, K. A.) 41–84 (Wiley, 2001).

72. Hudson, R. J. M. & Morel, F. M. M. Iron transport in marine-phytoplankton — kinetics of cellular and medium coordination reactions. *Limnol. Oceanogr.* **35,** 1002–1020 (1990).

73. Shaked, Y., Kustka, A. B. & Morel, F. M. M. A general kinetic model for iron acquisition by eukaryotic phytoplankton. *Limnol. Oceanogr.* **50,** 872–882 (2005).

74. Nodwell, L. M. & Price, N. M. Direct use of inorganic colloidal iron by marine mixotrophic phytoplankton. *Limnol. Oceanogr.* **46,** 765–777 (2001).

75. Strzepek, R. F. *et al.* Spinning the 'Ferrous Wheel': the importance of the microbial community in an iron budget during the FeCycle experiment. *Glob. Biogeochem. Cycles* **19,** GB4S26 (2005).

76. Barbeau, K., Moffett, J. W., Caron, D. A., Croot, P. L. & Erdner., D. L. Role of protozoan grazing in relieving iron limitation of phytoplankton. *Nature* **380,** 61–64 (1996).

77. Maranger, R., Bird, D. F. & Price, N. M. Iron acquisition by photosynthetic marine phytoplankton from ingested bacteria. *Nature* **396,** 248–251 (1998).

78. Sarthou, G. *et al.* The fate of biogenic iron during a phytoplankton bloom induced by natural fertilisation: Impact of copepod grazing. *Deep-Sea Res. II* **55,** 734–752 (2008).

79. Mioni, C. E., Poorvin, L. & Wilhelm, S. W. Virus and siderophore-mediated transfer of available Fe between heterotrophic bacteria: characterization using an Fe-specific bioreporter. *Aquat. Microb. Ecol.* **41,** 233–245 (2005).

80. Frew, R. D. *et al.* Particulate iron dynamics during FeCycle in subantarctic waters southeast of New Zealand. *Glob. Biogeochem. Cycles* **20,** GB1S93 (2006).

81. Lamborg, C. H., Buesseler, K. O. & Lam, P. J. Sinking fluxes of minor and trace elements in the North Pacific Ocean measured during the VERTIGO program. *Deep-Sea Res. II* **55,** 1564–1577 (2008).

82. Sunda, W. G. & Huntsman, S. A. Interrelated influence of iron, light, and cell size on marine phytoplankton growth. *Nature* **390,** 389–392 (1997).

83. Bowie, A. R. *et al.* The fate of added iron during a mesoscale fertilisation experiment in the Southern Ocean. *Deep-Sea Res. II* **48,** 2703–2743 (2001).

84. Chever, F., Sarthou, G., Bucciarelli, E., Blain, S. & Bowie, A. R. An iron budget during the natural iron fertilisation experiment KEOPS (Kerguelen Islands, Southern Ocean). *Biogeosciences* **7,** 455–468 (2010).

85. Weber, L., Völker, C., Schartau, M. & Wolf-Gladrow, D. A. Modeling the speciation and biogeochemistry of iron at the Bermuda Atlantic Time-series Study site. *Glob. Biogeochem. Cycles* **19,** GB1019 (2005).

86. Archer, D. E. & Johnson, K. S. A model of the iron cycle in the ocean. *Glob. Biogeochem. Cycles* **14,** 269–279 (2002).

87. Parekh, P., Follows, M. J. & Boyle, E. Modeling the global ocean iron cycle. *Glob. Biogeochem. Cycles* **18,** GB1002 (2004).

88. Gnanadesikan, A., Sarmiento, J. L. & Slater, R. D. Effects of patchy ocean fertilization on atmospheric carbon dioxide and biological production. *Glob. Biogeochem. Cycles* **17,** 1050 (2003).

89. Homoky, W. S., Severmann, S., Mills, R., Statham, P. & Fones, G. Pore-fluid Fe isotopes reflect the extent of benthic Fe redox recycling: evidence from continental shelf and deep-sea sediments. *Geology* **37,** 751–754 (2009).

90. Lacan, F. *et al.* Measurement of the isotopic composition of dissolved iron in the open ocean. *Geophys. Res. Lett.* **35,** L24610 (2008).

91. Kitayama, S. *et al.* Controls on iron distributions in the deep water column of the North Pacific Ocean: Iron(III) hydroxide solubility and marine humic-type dissolved organic matter. *J. Geophys. Res.* **114,** C08019 (2009).

92. Boyle, E. A., Bergquist, B. A., Kayser, R. A. & Mahowald, N. Iron, manganese, and lead at Hawaii Ocean Time-series station ALOHA: temporal variability and an intermediate water hydrothermal plume. *Geochim. Cosmochim. Acta* **69,** 933–952 (2005).

93. Borer, P. M., Sulzberger, B., Reichard, P. & Kraemer, S. M. Effect of siderophores on the light-induced dissolution of colloidal iron(III) (hydr) oxides. *Mar. Chem.* **93,** 179–193 (2005).

94. Croot, P. L., Streu, P. & Baker, A. R. Short residence time for iron in surface seawater impacted by atmospheric dry deposition from Saharan dust events. *Geophys. Res. Lett.* **31,** L23S08 (2004).

Acknowledgements

Additional information